MESOZOIC BACK-ARC EXTENSION IN THE ACTIVE MARGIN OF THE IRANIAN CONTINENTAL BLOCK: CONSTRAINTS FROM AGE AND GEOCHEMISTRY OF THE MAFIC LAVAS

Hadi Shafaii Moghadam*,°,✉, **Mohamad Rahgoshay**** and **Hubert Whitechurch***

* *Ecole et Observatoire des Sciences de la Terre, Institute de Physique du Globe, Strasbourg, France.*
** *Shahid Beheshti University, Faculty of Earth Sciences, Tehran, Iran.*
° *Damghan University of Basic Sciences, School of Earth Sciences, Damghan, Iran.*
✉ *Corresponding author, e-mail: hadi.shafaii@eost.u-strasbg.fr.*

Keywords: *ophiolites, calc-alkaline trend, island-arc tholeiitic trend, K-Ar age, back-arc extension. Nain-Baft, Iran.*

ABSTRACT

The Nain-Baft ophiolitic suture, along the active margin of the Central Iranian continental block (the Sanandaj-Sirjan zone) features back-arc extension during the Late Mesozoic. This ophiolitic belt is characterized by occurrence of mafic lavas including pillow lavas, diabasic dikes and layers, massive basaltic lavas and basaltic-andesitic rock fragments in the volcanic breccias. These mafic lavas display both calc-alkaline and island-arc tholeiitic affinities with enrichment in LILE and depletion in HFSE. Conventional K-Ar measurements on amphibole indicate the Middle Cretaceous for the creation and evolution of the Nain-Baft back-arc basins. As a result of oblique subduction of the Tethyan Ocean, a narrow transtensional back-arc basin could start to open along large transcurrent faults in the active margin of the Iranian continental block.

INTRODUCTION

The Upper Mesozoic geologic evolution of the Central Iranian continental block was dominated by the opening and extension of the Nain-Baft back-arc basin (Agard et al., 2006; Shafaii Moghadam et al., 2007). The Nain-Baft ophiolitic belt has been described as a tectonic mélange composed of blocks of oceanic origin (e.g., Davoudzadeh, 1972; Stocklin et al., 1972; Berberian and King, 1981; Desmons and Beccaluva, 1983; Arvin and Robinson, 1994; Arvin and Shokri, 1996). These complexes are organized as a pile of slices, stacked during the Late Cretaceous, crosscut by strike-slip faults. These slices comprise mantle peridotites (lherzolites, harzburgites and dunites), pegmatite gabbroic pockets, pillow lavas, basaltic-andesitic flows, amphibolites, diabasic dikes and layers, gabbro-norites, dacites, plagiogranites and cherts associated with pelagic limestones. The pieces of oceanic crust are covered by both Senonian limestones and also younger (Middle Paleocene to Early Eocene) transgressive detritic limy-sediments. The Nain-Baft ophiolitic belt has been interpreted as 1- a narrow oceanic basin, opened between the Lut block and the active margin of the Central Iranian block, the Sanandaj-Sirjan zone (e.g., Berberian and King, 1981; Davoudzadeh, 1972), 2- a Cretaceous arc basin related to the Tethyan subduction (e.g., Desmons and Beccaluva, 1983), 3- the Upper Cretaceous Nain-Baft back-arc basin (e.g., Shahabpour, 2005; Agard et al., 2006). In this study we will focus i) on the geochemical signature of mafic lavas in the Nain-Baft ophiolites (including Nain, Dehshir, Shahr-e-Babak and Baft complexes), ii) on dating more precisely the crystallization age of these ophiolites, iii) on proposing a consistent eruptive environment for these ophiolites.

TECTONIC HISTORY OF THE CENTRAL IRANIAN CONTINENTAL BLOCK

The tectonic history of the Central Iranian block began with the detachment of the Mega-Lhasa block (Ricou, 1994) from Gondwana during Permian-Triassic. Collision of the Central Iranian block with Eurasia (Turan Plate) took place in the Middle Triassic during the early Cimmerian phase. As soon as the continental collision between Central Iranian block and Eurasia was accomplished, subduction of Neo-Tethys started south of the Central Iranian block in Late Triassic-Early Jurassic times. This subduction caused the Sanandaj-Sirjan zone to became an active continental margin of the Central Iranian block (Fig. 1), as evidenced by the occurrence of Mesozoic calc-alkaline lavas and plutons (Berberian and Berberian, 1981; Berberian and King, 1981). Reconstruction of the Tethyan realm suggests an oblique subduction (Berberian and King, 1981; McClay et al., 2004), with fundamental changes during the Late Cretaceous, following the exhumation of blueschists from the Esfandagheh region (Agard et al., 2006).

FIELD OCCURRENCE AND MINERAL ASSEMBLAGE OF THE MAFIC LAVAS

The Nain ophiolites are characterized by occurrence of pillow lavas and diabasic dikes. In places, pillow lavas are overlain stratigraphically by cherts and reddish siliceous limestones of Maastrichtian age. Diabasic dikes occur both as dike swarm complex and as isolated dikes, crosscutting the mantle peridotites. Clinopyroxene ($Wo_{31-41}En_{57-48}Fs_{12-11}$) (Table 1) and plagioclase (An_{71-73}) (Table 2) phenocrysts associated with plagioclase microlites are the main primary constituents of pillow lavas. In the diabasic dikes clinopyroxene grains ($Wo_{42-37}En_{47-49}Fs_{11-14}$) are segregated between plagioclase microlites and chloritized amphiboles (actinolite

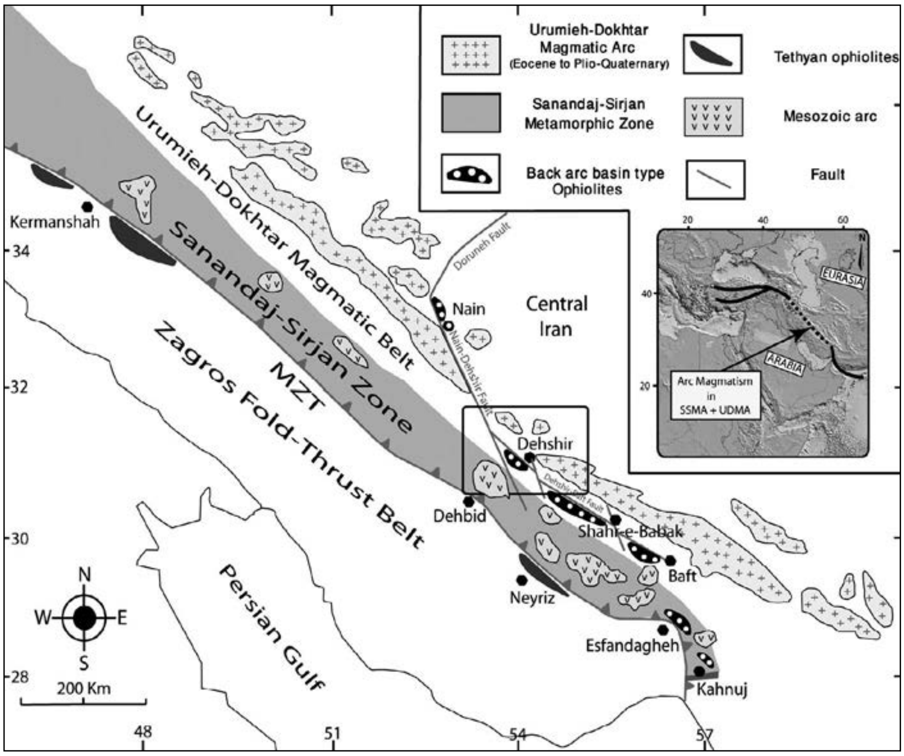

Fig. 1 - Schematic map showing the distribution of the Nain-Baft ophiolites and the alignment of the Urumieh-Dokhtar, Eocene - Plio-Quaternary magmatic arc, and the Mesozoic arc of the Sanandaj-Sirjan zone.

Table 1 - Representative composition of clinopyroxene grains in the Nain-Baft mafic rocks.

Massif Rock-type Sample	Nain diab. dike BS05-16	Nain pillow lava BPV-2	Dehshir diab. dike AZ06-29	Dehshir pillow lava AZ06-2	Sh.Babak pillow lava R06-4	Sh.Babak basalt R06-32	Sh.Babak diabase R06-14	Baft and.frag BT06-10	Baft and.frag BT06-10	Baft bas.flow BT06-15
SiO2	51.76	51.49	52.28	50.7	52.36	50.07	47.58	52.85	53.13	51.97
TiO2	0.26	0.77	0.36	0.29	0.56	0.51	1.25	0.3	0.36	0.24
Al2O3	2.9	4.38	1.99	2.26	3.08	4.26	7.53	0.95	2.12	2.3
FeO	8.48	6.77	7.95	8.11	6.13	8.66	9.04	10.16	18.56	5.27
Cr2O3	0	0.63	0.1	0.28	0.19	0.08	0.06	0	0.01	0.62
MnO	0.2	0.14	0.2	0.38	0.13	0.25	0.21	0.43	0.55	0.18
NiO	0.09	0	0.16	0	0.05	0.03	0	0.07	0	0.01
MgO	17.27	16.5	16.85	18.79	15.62	13.82	12.32	14.23	22.54	16.09
CaO	18.13	19.62	18.45	17.96	22.49	21.39	21.88	20.91	2.09	21.34
Na2O	0.15	0.19	0.29	0.27	0.17	0.35	0.25	0.34	0.02	0.16
K2O	0.04	0.02	0.02	0	0	0	0	0.03	0	0
Total	99.28	100.53	98.65	99.03	100.8	99.43	100.12	100.25	99.38	98.2

Table 2 - Representative composition of plagioclase grains in mafic rock units of the Nain-Baft ophiolites.

Rock-type Massif Sample	pillow lava Nain BPV-2	pillow lava Nain BPV-2	pillow lava Dehshir AZ06-2	basalt Sh.Babak R06-32	basalt Sh.Babak R06-32	and.fragm Baft BT06-10	and.fragm Baft BT06-10
SiO2	50.3134	50.0039	66.053	53.88	49.606	45.177	56.719
TiO2	0.0509	0.0002	0.062	0	0.037	0.068	0.075
Al2O3	30.1065	29.8015	21.3	27.376	29.556	34.907	26.441
FeO	0.5716	0.3734	0.418	0.449	0.78	0.612	0.768
MnO	0.0002	0.0627	0.018	0	0	0	0.031
MgO	0.3139	0.2804	0.03	0.066	0.101	0.041	0.066
CaO	14.6143	14.9777	2.372	11.346	14.865	18.472	8.555
Na2O	3.2403	3.0037	10.592	4.61	2.997	0.976	6.414
K2O	0.0001	0.0049	0.563	0.405	0.3	0.007	0.369
Total	99.2112	98.5084	101.41	98.13	98.24	100.26	99.44

to magnesio hornblende) (Table 3).

In the Dehshir ophiolites, the mafic rocks are characterized by the presence of pillow lavas, diabasic dikes and massive lava flows. Pillow lavas (and massive basalts) are stratigraphically overlain by cherts and/or show fault contacts with a dike (dacitic-andesitic) swarm complex. Diabasic dikes occur isolated, crosscutting the peridotites, the gabbros and even the pillow lavas. Clinopyroxene ($Wo_{35-45}En_{52-41}Fs_{13-14}$) (Table 1) and highly sericitized-albitized (Ab_{86-99}) (Table 2) plagioclases are the main rock-forming minerals of pillow lavas. In the diabasic dikes, plagioclase laths are dominant, altered into clay minerals and epidote. Clinopyroxens ($Wo_{38-43}En_{47-44}Fs_{15-12}$) display alteration into euralite and chlorite.

Table 3 - Representative composition of amphibole grains in the Nain-Baft mafic rocks.

Massif	Nain	Nain	Sh.Babak	Sh.Babak
Sample	BS05-16	BS05-16	R06-14	R06-14
Rock type	diab.dike	diab.dike	diabase	diabase
SiO2	52.892	46.347	39.795	41.924
TiO2	0.076	0.678	2.912	2.167
Al2O3	3.218	2.701	13.598	11.552
FeO	11.374	12.648	15.766	15.132
Cr2O3	0	0	0	0.006
MnO	0.128	0.492	0.336	0.316
MgO	14.147	14.441	10.675	12.227
CaO	12.688	16.283	10.7	10.817
Na2O	0.201	0.567	2.356	2.259
K2O	0.046	0.16	0.754	0.677
Total	94.77	94.317	97.24	97.48

Magmatism in the Shahr-e-Babak ophiolites is bimodal, with predominant basalt (pillow lavas, basaltic flows or layers and diabasic layers) and rhyolite, and negligible occurrence of andesite and trachyandesite. Pillow lavas occur as small, local outcrops and in places alternated with thin pelagic limestone and/or chert layers. Basaltic sheet flows are either intercalated with pillow lavas and/or interbedded with rhyolitic-diabasic layers. Moreover, diabasic rocks are found as layers with various thicknesses, alternated with basaltic, andesitic and pelagic limestone layers. Plagioclase and clinopyroxene phenocrysts ($Wo_{38}En_{48}Fs_{14}$ to $Wo_{46}En_{44}Fs_{10}$), along with plagioclase microlites are the main primary constituents of pillow lavas. Moreover, the basaltic flows have clinopyroxene grains ($Wo_{45}En_{40}Fs_{15}$ to $Wo_{42}En_{41}Fs_{16}$) segregated between plagioclase (An_{56-72}) laths. In diabasic layers, plagioclase microlites are the dominant phase, and show alteration into sericite and clay minerals, while clinopyroxene grains ($Wo_{47}En_{37}Fs_{16}$ to $Wo_{42}En_{49}Fs_{9}$) are occasionally found in a less altered state. Pargasite is the other rock-forming phase of these diabasic layers (Table 3).

In addition to pillow lavas and diabasic dikes, volcanic breccias with basaltic-andesitic fragments, alternating with basaltic layers are common in the Baft ophiolites. The basaltic-andesitic fragments consist of uralitized clinopyroxenes ($Wo_{42}En_{41}Fs_{18}$ to $Wo_{43}En_{40}Fs_{17}$) (Table 1), minor amounts of orthopyroxene ($Wo_{4}En_{65}Fs_{31}$ to $Wo_{7}En_{53}Fs_{40}$) and plagioclases. Plagioclases form lath-shaped phenocrysts with oscillatory zoning (An_{42-91}) (Table 2) and/or groundmass microlites. Basaltic layers have clinopyroxenes ranging in composition from $Wo_{44}En_{47}Fs_{9}$ to $Wo_{40}En_{49}Fs_{11}$ (Table 1).

ANALYTICAL METHODS

The ICP-MS and ICP-AES analyses were performed at the "Centre de Geochimie de la surface", Strasbourg (France). About 1 g of agate-crushed sample was dried first at 110°C and then charred at 1000°C for 3 hours. Afterwards, 100 mg of the charred sample was mixed with 750 mg of lithium tetraborate in the graphite furnace. This mixture was melted at 1000°C for 30 minutes. After cooling, the obtained bead was directly dissolved in furnace by a solvent containing diluted nitric acid and glycerin. The final solution is 4g/l (100 mg of rock in 25 ml of solvent), after filtering directly entered into ICP-AES. The same solution, diluted 10 times, was entered into ICP-MS. In this way, major elements and Ni, Cr, V, Sc, Y, Zr, Ba, Sr were measured by ICP-AES, whereas other trace and rare earth elements were determined by the ICP-MS technique. Otherwise, the composition of minerals in the mafic lavas of the Nain-Baft ophiolites were measured by a Cameca SX-50 in Paris VI University. For this purpose, the accelerating voltage and beam current were 12keV and 10nA respectively. On the other hand, K-Ar measurements were performed in Ecole et Observatoire des Sciences de la Terre (Strasbourg) following method described by Montigny (1989).

GEOCHEMISTRY OF THE MAFIC LAVAS

Some of the analyzed samples have a high loss on ignition (Table 4), indicating alteration and high volatile contents. Otherwise, Na_2O values also show high concentration in some samples, a characteristic feature of spilitic basalts. Hydrothermal ocean floor metamorphism affected the Nain-Baft ophiolite belt to various degrees. The distribution of hydrous assemblages during spilitization, is thought to predominantly reflect ocean floor processes. The effect of hydrothermalism on the geochemistry of the mafic samples was evaluated by plotting various elements against the immobile element zirconium (not shown). The mafic lavas show good correlations against zirconium for all elements except for Na_2O, CaO, FeO_t, Rb, Sr, K, Pb and Cs. Nonetheless, despite the relatively consistent behaviour of the large ion lithophile elements, we mostly use immobile trace elements (such as REE and HFSE) for the paleotectonic interpretation of the mafic lavas.

Using the LOI versus Na_2O and SiO_2 diagrams (not shown) we selected the samples with less than 4% LOI to avoid alteration effect. In $Na_2O + K_2O$ against SiO_2 diagram (Le Bas et al., 1986) most rocks plot in the basalt, basaltic andesite, trachybasalt and basaltic trachyandesite fields (Fig. 2). The exceptions are two pillow lavas from the Dehshir (61.5 SiO_2%wt) and the Baft (60.8 SiO_2%wt) ophiolites, with andesite and trachyandesite compositions. Most mafic lavas of the Nain-Baft ophiolites are characterized by considerable low TiO_2 contents and in TiO_2 versus FeO_t/MgO diagram cover the IAT (Island-arc tholeiite) field (Fig. 3).

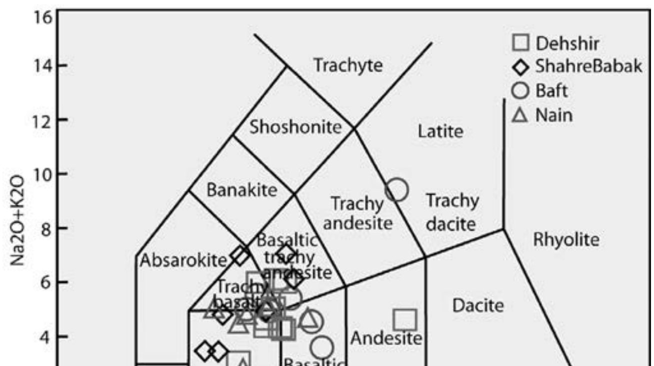

Fig. 2 - Classification of the mafic rock units of the Nain-Baft suture in $Na_2O + K_2O$ against SiO_2 diagram (TAS diagram) of Le Bas et al. (1986). In this diagram, we have selected the mafic samples with less than 4% LOI for plotting.

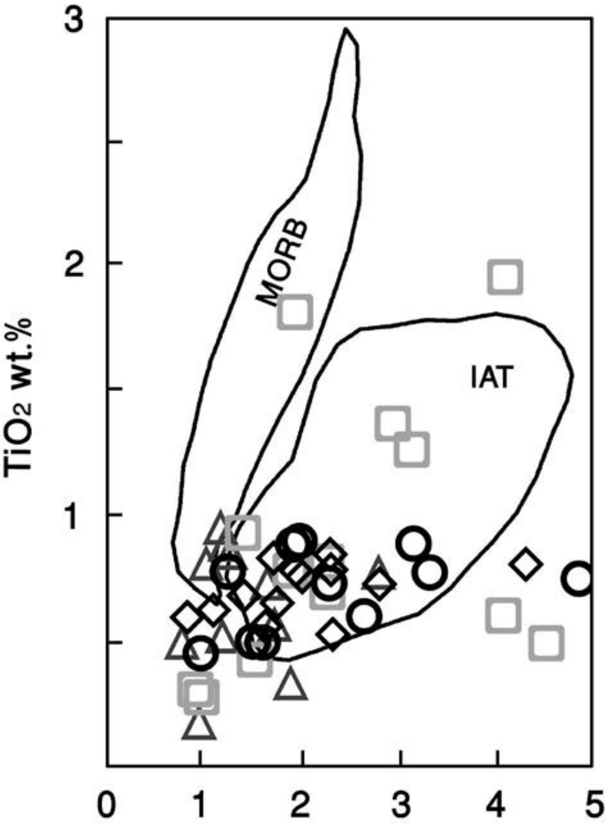

Fig. 3 - TiO_2 versus FeO_t/MgO diagram for discriminating the mafic lavas of the Nain-Baft ophiolitic belt.

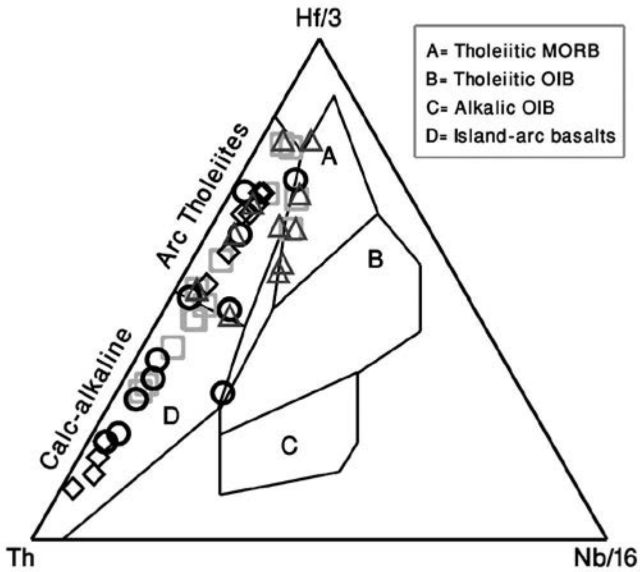

Fig. 4 - Hf-Th-Nb discriminative diagram (Wood, 1980) documents the affinity of the mafic rocks to fall in the field of island-arc basalts.

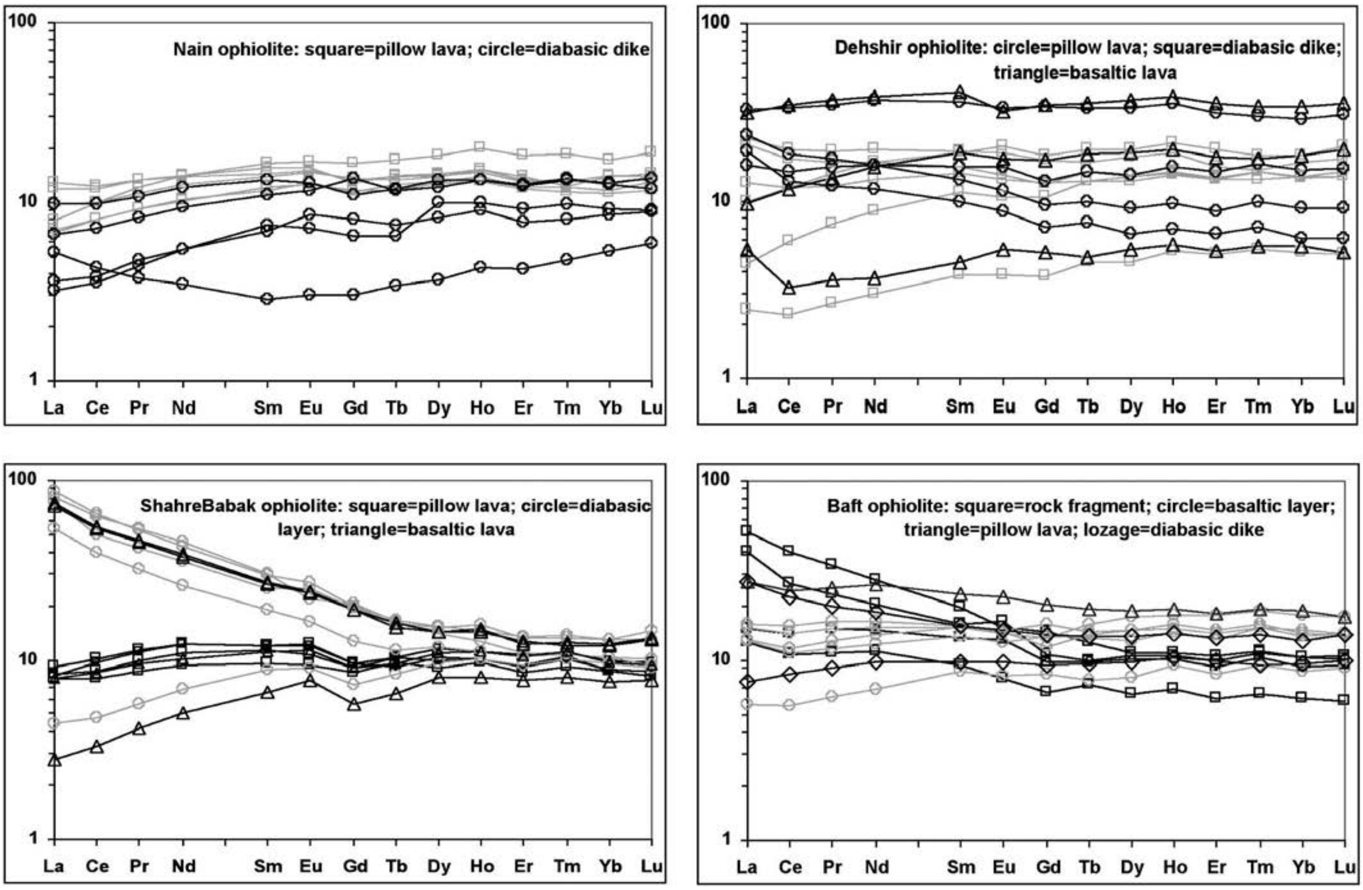

Fig. 5 - Geochemistry of the rock units of the Nain-Baft suture based on the chondrite-normalized REE patterns (normalized values from McDonough and Sun, 1995).

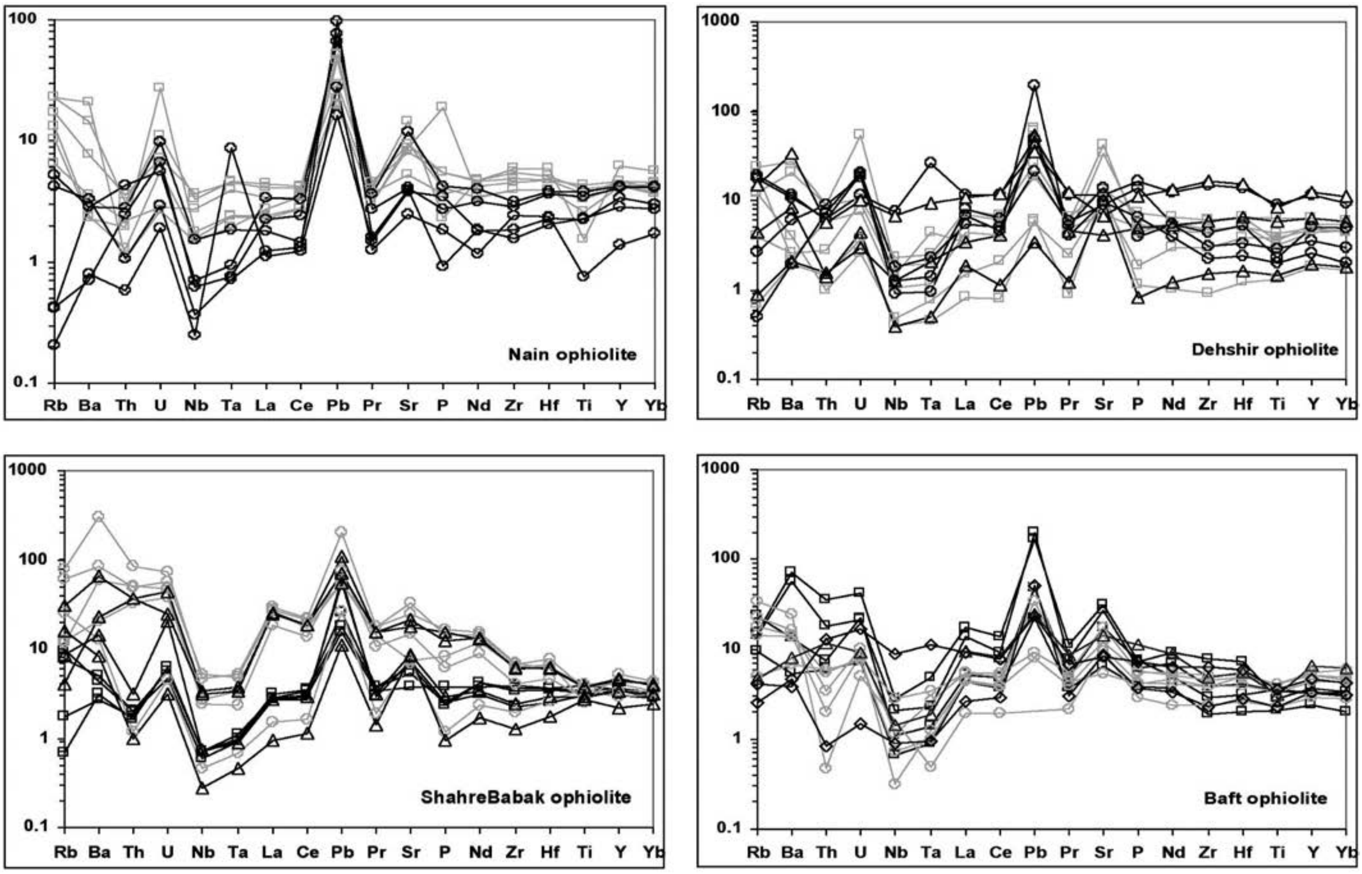

Fig. 6 - Geochemistry of the rock units of the Nain-Baft suture based on the primary mantle-normalized trace elements patterns (normalized values from McDonough and Sun, 1995).

On the basis of trace element composition and Th-Hf-Nb diagram of Wood (1980), the Nain basaltic rocks fall in the arc tholeiitic field (and/or in N-MORB field), whereas the mafic lavas of the Dehshir, Shahr-e-Babak and Baft ophiolites show tendency to plot in both the arc tholeiites and calc-alkaline fields (Fig. 4). The most striking feature of this diagram is the strong calc-alkaline signature of the Baft and Shahr-e-Babak lavas.

Chondrite-normalized (McDonough and Sun, 1995) REE patterns for the Nain pillow lavas are relatively flat with slight LREE depletion ($La_{(N)}/Yb_{(N)} = 0.48$-0.89). Most of the diabasic dikes have relatively low contents of bulk REE (Fig. 5). They feature flat or slightly LREE depleted pattern. When the ≤incompatible elements are taken into account for these mafic lavas, they display enrichment in Ba, Rb, U, Pb, K and Sr and depletion in Nb, Ta, Th and Ti (Fig. 6).

The Dehshir pillow lavas, diabasic dikes and basaltic massive lavas are characterized by both flat pattern and differentiated pattern with LREE depletion, indicating the different degree of partial melting (Fig. 5). The bulk REE content varies from considerable low to high concentrations, consistent with fractional crystallization and/or two melting stages of the mantle source(s). Depletion in HFSE is a prominent feature of the Dehshir lavas. Two samples of pillow lavas (A06-2 and A06-3 samples) show enrichment in LREE along with depletion in Nb, Ti, and enrichment in Pb, U, and Th, showing the calc-alkaline signature (Fig.6).

Three different types of patterns can be observed in the chondrite-normalized diagram of the mafic lavas of the Shahr-e-Babak ophiolites. i)- differentiated patterns with strong LREE enrichment (basaltic lavas and diabasic layers). ii)- flat patterns characteristic of pillow lavas and one of basaltic massive lavas (R06-24). iii)- LREE depletion for basaltic lavas and diabasic layers (Fig. 5). All these rocks are depleted in HFSE and show enrichment in LILE. Therefore, two distinct types of lavas are recognized: lavas with IAT affinity and lavas with calc-alkaline properties.

The mafic lavas in the Baft ophiolites are characterized by both flat patterns (especially for the basaltic layer) and LREE enriched patterns (for the rock fragment in volcanic breccia, pillow lavas and diabasic dikes), suggesting IAT and calc-alkaline geochemical signatures respectively (Fig. 5). Enrichment in Pb, U, Ba, Rb, Sr, K (and Th for the calc-alkaline series) and depletion in Nb, Ta, Ti are the special properties of these lavas (Fig. 6).

As mentioned above, all mafic lavas in the Nain-Baft ophiolites are of calc-alkaline and/or island-arc tholeiitic affinities, as marked particularly by enrichment in LILE and depletion in HFSE. It is noteworthy that the higher degree of LILE enrichment (high LILE/HFSE ratio) is consistent with partial melting of a subduction-contaminated mantle wedge (McCulloch and Gamble, 1991; Saunders and Tarney, 1991; Taylor and Martinez, 2003). Furthermore, depletion in Nb, Ta and Ti is ascribed to arc-derived lavas (e.g., Hawkesworth et al., 1991; McCulloch and Gamble, 1991). Geochemically, lavas from the Nain-Baft show similarity to lavas erupted in back-arc basin environments, such as the Mariana Trough (Stern et al., 1990) and/or the Lau basin (Frenzel et al., 1990). Different degrees of partial fusion along with melting of different mantle sources are supposed to be responsible for generating LREE depleted, flat and/or LREE enriched patterns.

Table 4 - Whole rock composition of mafic rock units of the Nain-Baft ophiolites.

Rock	d.dike	d.dike	d.dike	d.dike	d.dike	pillow	pillow	pillow	b.lava	b.lava	b.frag	b.frag	and.frag	and.frag	b.lava	b.lava	b.layer	b.layer	b.layer	pillow	d.dike	d.dike	pillow	pillow
Locality	Dehshir	Dehshir	Dehshir	Dehshir	Dehshir	Dehshir	Dehshir	Dehshir	Dehshir	Dehshir	Baft	Baft	Baft	Baft	Baft	Baft	Baft	Baft	Baft	Baft	Baft	Baft	Sh.Babak	Sh.Babak
Sample	A06-1	AZ06-29	G06-16	DAR05-3	DZ05-4	A06-2	A06-3	AZ06-32	DAR05-5	D06-10	BT06-36	BT06-8	BT06 - 10	BT06-18	BT06 - 15	BT06-13	BT06-17	BT06 - 16	BT06 - 19	BT06-38	BT05-10	BT05-2A	R06-2	R06-4
SiO2	51.7	48.7	52.2	52.2	51.8	46.9	45.4	61.5	48.8	50.5	43.9	47.6	55.1	57.0	49.4	53.4	54.4	51.2	50.1	60.8	40.3	52.7	44.5	53.2
Al2O3	15.5	14.1	15.0	13.9	14.6	10.8	13.9	15.5	13.1	14.6	17.1	18.7	18.2	10.6	19.0	13.4	14.7	17.1	16.8	16.0	11.1	15.9	13.4	13.5
TiO2	0.934	0.285	0.822	0.775	0.694	0.438	0.615	0.500	1.26	0.317	0.775	0.753	0.607	0.458	0.503	0.893	0.884	0.902	0.731	0.669	0.5012	0.776	0.697	0.738
FeOt	10.0	9.35	10.6	10.2	9.87	9.15	10.5	6.84	11.7	8.87	10.6	10.3	8.22	6.87	6.87	12.7	11.3	10.44	10.89	7.85	7.75	6.99	7.89	7.42
MnO	0.158	0.108	0.173	0.164	0.139	0.153	0.148	0.197	0.185	0.148	0.182	0.223	0.156	0.143	0.145	0.169	0.159	0.140	0.155	0.218	0.126	0.111	0.124	0.149
MgO	7.20	9.64	4.75	5.45	4.39	6.06	2.59	1.53	3.76	9.80	3.20	2.15	3.11	7.13	4.34	4.05	5.87	5.38	4.77	1.28	5.06	5.67	5.69	2.67
CaO	4.99	12.7	8.22	9.76	9.27	13.9	12.7	6.76	14.6	9.57	12.5	11.3	8.34	9.48	9.02	6.51	6.20	6.62	7.58	2.54	27.2	8.7	16.1	13.1
Na2O	4.40	1.38	5.20	3.79	5.23	4.60	5.88	4.58	3.1	2.14	4.03	3.29	3.34	2.01	3.32	3.28	3.59	3.84	3.33	8.96	1.64	5.12	4.28	4.31
K2O	1.39	0.061	0.816	0.58	0.82	0.713	0.145	0.042	0.004	0.221	1.14	0.508	0.25	0.586	1.68	0.256	0.960	1.09	2.15	0.378	0.05	0.29	0.049	0.612
P2O5	0.096	0.025	0.040	0.16	0.12	0.141	0.302	0.087	0.108	0.018	0.162	0.133	0.160	0.085	0.063	0.088	0.125	0.119	0.092	0.246	0.08	0.16	0.052	0.054
LOI	2.41	2.73	1.03	2.21	1.96	5.85	7.13	1.66	2.23	2.72	7.19	5.20	1.06	4.64	4.74	4.82	2.32	2.66	2.63	1.22	5.21	2.37	6.94	4.44
Total	98.80	99.10	98.95	99.24	98.98	98.68	99.24	99.17	98.89	98.90	100.67	100.20	98.55	99.05	99.09	99.52	100.48	99.50	99.20	100.16	99.02	98.82	99.72	100.16
Ba	192	13.6	27.3	143	15.35	81.8	42.3	13.4	14.5	59	92.4	393	503	37.8	168	47.5	97.2	114	100	57	33	27	18.7	30.6
Sc	36.9	47.0	24.5	34	31	49.4	37.9	16.9	34	41	35.7	27.2	20	24.6	32	38.2	40.5	41	43	32	32	32	33.2	26.1
V	281	236	297	237	293	360	291	98.1	359	199	259	244	160	193	254	403	358	352	372	144	237	220	241	323
Cr	110	299	14.1	82	62	580	38.1	6.12	32.8	530	24.2	-	5	311	138	6.77	9.95	27	24	-	105	23	296	23.3
Ni	58.7	94.6	36.0	32	41	211	27.3	4.89	16.1	109	4.57	13.4	12	106	55	11.0	23.3	23	32	6	37	36	87.8	26.2
Rb	15.2	0.438	7.51	8	12.6	12.1	1.68	0.312	0.563	2.79	15.1	9.13	9.84	6.10	21.9	3.13	9.19	14.7	11.43	2.96	1.62	2.57	1.12	6.37
Sr	869	272	211	279	701	204	187	288	85.4	209	367	563	661	140	202	113	250	372	212	299	183	176	135	112
Y	22.6	8.15	21.8	25	19.9	11.8	16.0	23.4	28.4	9	14.5	14.6	17	10.8	13	25.5	23.2	24	20	29	15	21	13.9	16.6
Zr	52.5	10.4	33.2	68.2	49.3	25.3	33.9	50.2	65.9	17	32.4	42.9	87	21.3	26	42.6	51.5	58	42	54	26	72	38.0	41.0
Nb	1.353	0.288	0.346	1.65	0.758	0.656	0.908	1.290	0.888	0.277	0.777	1.494	2.05	0.474	-	0.515	2.04	0.807	0.223	1.03	0.641	6.35	0.498	0.514
Cs	7.43	0.020	0.107	0.028	0.534	0.631	0.287	0.078	0.361	0.182	4.79	0.660	9.53	0.135	0.577	0.130	0.146	0.501	0.322	0.002	0.521	0.02	0.089	0.141
La	4.89	0.572	1.04	5.36	2.99	4.57	5.57	3.78	2.32	1.27	3.53	9.59	12.2	2.99	1.36	3.13	3.65	3.76	3.06	6.49	1.8	6.42	2.18	1.93
Ce	10.6	1.41	3.64	12.1	7.24	8.01	11.2	9.03	7.15	2.00	8.73	16.4	24.6	6.58	3.44	7.13	8.75	9.48	6.79	14.8	5.17	13.9	6.22	5.92
Pr	1.55	0.245	0.691	1.78	1.14	1.14	1.59	1.45	1.26	0.335	1.39	2.17	3.11	1.02	0.588	1.19	1.39	1.52	1.09	2.36	0.844	1.85	1.05	1.03
Nd	7.54	1.36	4.01	8.91	6.08	5.39	7.33	7.33	7.14	1.68	6.71	9.43	12.6	5.09	3.19	6.32	7.06	7.57	5.61	12.0	4.48	8.51	5.59	5.58
Sm	2.31	0.566	1.65	2.86	2.14	1.47	1.94	2.30	2.76	0.672	1.98	2.36	2.92	1.40	1.30	2.27	2.26	2.31	2.00	3.48	1.46	2.31	1.77	1.77
Eu	0.797	0.214	0.599	1.05	0.74	0.492	0.643	0.869	0.978	0.300	0.745	0.924	0.858	0.449	0.467	0.798	0.808	0.835	0.717	1.270	0.552	0.826	0.689	0.672
Gd	2.48	0.742	2.086	3.38	2.53	1.425	1.890	2.59	3.39	1.015	1.95	2.14	2.85	1.331	1.66	2.67	2.37	3.18	2.71	4.055	1.87	2.77	1.88	1.89
Tb	0.524	0.161	0.468	0.602	0.465	0.273	0.358	0.531	0.662	0.172	0.351	0.362	0.452	0.264	0.280	0.571	0.497	0.517	0.479	0.703	0.348	0.495	0.330	0.373
Dy	3.35	1.11	3.17	4.33	3.39	1.63	2.25	3.42	4.64	1.31	2.51	2.62	2.69	1.62	1.99	4.32	3.61	3.59	3.14	4.64	2.42	3.38	2.55	2.82
Ho	0.794	0.284	0.772	1.02	0.782	0.384	0.528	0.857	1.07	0.309	0.556	0.584	0.602	0.375	0.516	0.970	0.822	0.869	0.788	1.06	0.565	0.777	0.550	0.602
Er	2.16	0.794	2.12	2.52	2.11	1.04	1.41	2.34	2.8	0.827	1.48	1.62	1.69	0.993	1.35	2.83	2.26	2.34	2.11	2.94	1.6	2.15	1.50	1.70
Tm	0.377	0.137	0.376	0.383	0.34	0.183	0.250	0.418	0.442	0.143	0.267	0.282	0.285	0.167	0.239	0.483	0.387	0.408	0.390	0.495	0.24	0.351	0.267	0.278
Yb	2.15	0.831	2.23	2.66	2.23	0.994	1.47	2.41	2.9	0.902	1.49	1.67	1.67	1.001	1.41	2.89	2.35	2.27	2.18	3.04	1.56	2.09	1.40	1.58
Lu	0.341	0.124	0.341	0.425	0.358	0.152	0.223	0.376	0.483	0.126	0.234	0.259	0.252	0.145	0.223	0.435	0.351	0.342	0.346	0.433	0.244	0.345	0.203	0.238
Hf	1.59	0.371	1.18	1.98	1.6	0.749	1.03	1.64	1.99	0.506	0.962	1.28	2.23	0.626	0.803	1.53	1.50	1.58	1.24	1.72	0.868	1.84	1.08	1.12
Ta	0.079	0.018	0.031	0.103	0.049	0.039	0.058	0.094	0.084	0.020	0.056	0.094	0.198	0.037	0.020	0.040	0.141	0.106	0.051	0.077	0.039	0.467	0.041	0.038
Pb	1.32	0.429	0.404	1.84	4.16	13.7	3.00	1.53	3.81	0.246	3.38	13.8	11.8	1.54	-	3.47	2.47	0.656	0.564	1.75	3.64	1.69	1.80	1.27
Th	0.772	0.123	0.085	0.757	0.496	0.522	0.766	0.609	0.135	0.118	0.631	1.52	3.04	0.509	0.040	0.510	0.470	0.291	0.169	0.980	0.072	1.1	0.148	0.171
U	1.1	0.076	0.055	0.216	0.157	0.408	0.381	0.423	0.063	0.091	0.471	0.445	0.885	0.153	0.107	0.160	0.167	0.215	0.183	0.194	0.031	0.358	0.130	0.115

Abbreviations: d.dike = diabasic dike: b.lava = basaltica lava; b.frag = basaltic fragment; and.frag = andesitic frag; b.layer = basaltic layer; d.layer = diabasic layer.

Table 4 (*continued*)

Rock	pillow	pillow	d.layer	d.layer	d.layer	d.layer	d.layer	b.lava	b.lava	b.lava	b.lava	pillow	pillow	pillow	pillow	pillow	pillow	d.dike	d.dike	d.dike	d.dike	d.dike
Locality	Sh.Babak	Sh.Babak	Sh.Babak	Sh.Babak	Sh.Babak	Sh.Babak	Sh.Babak	Sh.Babak	Sh.Babak	Sh.Babak	Sh.Babak	Nain	Nain	Nain	Nain	Nain	Nain	Nain	Nain	Nain	Nain	Nain
Sample	R06-1	R06-3	R06-9	R-05-6	R06-45	R06-14	R06-47	R06-24	R-05-10A	R-05-10B	R06-32	BAH-35	BAH-36	BF-4	BF2	BPV2	BS05-3	BAH-14	BS05-13	BS05-16	BSU-10	BSU-11
SiO_2	46.7	47.4	47.5	53.7	48.8	46.4	47.1	47.4	53.1	52.4	50.9	48.9	47.1	28.1	44.7	49.4	49.1	53.4	41.9	51	46.3	54.2
Al_2O_3	12.6	13.0	17.1	15.8	15.6	13.7	17.8	16.0	16.1	16.4	14.3	15.6	15.8	19.4	16.7	16.5	15.3	14.1	10.1	14.7	12.1	12.8
TiO_2	0.835	0.665	0.792	0.544	0.775	0.618	0.865	0.637	0.807	0.816	0.577	0.867	0.937	0.559	0.724	0.329	0.797	0.751	0.164	0.507	0.491	0.84
FeOt	7.59	9.98	11.7	5.06	10.40	9.61	11.5	10.6	7.49	7.44	12.1	8.78	8.72	8.16	8.93	10.2	7.69	9.9	6.42	8.91	6.66	9.38
MnO	0.109	0.150	0.212	0.078	0.169	0.189	0.183	0.148	0.192	0.074	0.163	0.135	0.136	0.13	0.159	0.172	0.139	0.145	0.095	0.207	0.158	0.191
MgO	4.47	5.76	6.11	2.18	5.29	11.5	5.04	9.71	3.28	1.75	7.49	7.26	7.52	4.73	5.44	5.4	7.54	3.57	6.77	7.52	8.71	7.46
CaO	14.8	13.1	7.06	8.25	7.89	10.00	6.03	9.23	6.92	8.25	7.21	9.74	9.86	15	13.2	9.64	13.6	13.1	29	7.88	22	8.15
Na_2O	4.84	3.34	2.99	6.89	3.90	2.58	4.34	2.78	4.87	6.82	4.10	3.56	3.53	15.89	3.38	3.75	2.51	0	0.25	4.51	0.198	4.2
K_2O	0.030	0.266	1.79	0.822	3.07	0.846	2.90	0.603	1.24	0.225	0.793	0.79	1.34	2.2	0.49	0.84	0.25	0	0.01	0.522	0	0.342
P_2O_5	0.081	0.055	0.026	0.180	0.309	0.137	0.362	0.064	0.271	0.335	0.020	0.12	0.12	0.41	0.09	0.05	0.08	0.06	0.04	0.02	0.075	0.093
LOI	6.73	4.88	4.52	5.40	3.63	4.25	3.05	2.46	4.06	3.83	1.52	3.22	4.14	4.76	5.23	2.66	1.86	4.25	4.12	2.91	2.62	2.05
Total	98.77	98.60	99.77	98.90	99.76	99.77	99.09	99.62	98.33	98.30	99.22	99.01	99.18	99.39	98.98	98.89	98.9	99.26	98.85	98.65	99.3	99.63
Ba	21.8	35.0	90.2	144	2124	415	604	100	468	159	58.4	54	102	16	17	145	25	5	20	23.3	5.63	20.1
Sc	40.1	44.1	39.8	15.4	24.8	28.9	29	36.6	23.3	23.8	49.1	41	43	38	39	43	37	34	34	41.6	28.2	33
V	236	308	349	203	234	213	265	275	246	330	357	232	235	249	249	288	228	411	196	264	179	263
Cr	186	233	1.21	1.90	88.6	978	-	65.5	30.6	55.2	39.2	236	257	566	572	194	331	6	231	177	238	192
Ni	63.8	68.5	8.14	5.53	28.3	196	10	35.6	18.1	18.8	14.2	79	91	122	126	61	119	29	54	56	82.1	61.9
Rb	0.439	4.94	16.2	8.01	50.3	7.27	38.4	5.47	19.7	2.57	10.2	10.9	14.7	6.53	8.41	14.6	4.19	0.271	0.262	2.68	0.13	3.35
Sr	80.3	153	149	156	696	319	514	179	449	373	178	170	198	184	199	302	112	86	52	83.2	81.4	252
Y	16.1	15.7	13.2	23.4	18.9	15.1	18	15.1	20.6	21.3	9.94	19.9	21	19	19	28	21.1	18.9	6.39	13	15.5	19.4
Zr	43.9	24.9	21.6	69.3	76.4	45.1	78	26.8	66.3	69.3	14.3	61.1	55	44	44	67	50.3	32.5	27.4	17.5	20.8	35
Nb	0.499	0.425	0.324	1.93	3.36	1.758	3.74	0.517	2.27	2.36	0.200	2.63	2.39	1.26	1.13	1.07	1.93	0.45	1.09	0.261	0.179	0.505
Cs	0.071	0.081	6.37	0.049	0.384	0.211	0.005	0.253	0.129	0.070	0.183	0.391	0.597	0.172	0.203	0.386	0.114	0.019	0.037	0.032	ND	0.172
La	1.96	1.85	1.05	18.0	20.6	12.7	19.2	1.87	17.9	17.2	0.655	2.8	3.02	1.65	1.58	1.86	2.31	1.56	1.24	0.852	0.764	2.31
Ce	5.31	4.80	2.89	30.5	40.0	24.2	38.5	5.20	33.4	32.8	2.01	7.3	7.55	4.93	4.91	6.11	6.03	4.35	2.62	2.36	2.17	5.96
Pr	0.924	0.803	0.527	3.90	4.91	2.97	5.00	0.881	4.33	4.19	0.385	1.24	1.24	0.849	0.844	1.12	1.04	0.756	0.348	0.443	0.408	1
Nd	5.02	4.25	3.12	16.2	19.7	12.0	20.8	4.61	17.9	17.3	2.31	6.43	6.32	4.66	4.64	6.39	5.67	4.27	1.59	2.5	2.46	5.46
Sm	1.68	1.40	1.31	3.68	4.43	2.83	4.51	1.64	4.00	3.92	0.986	2.31	2.12	1.7	1.77	2.43	2.05	1.62	0.419	1.02	1.1	1.95
Eu	0.602	0.528	0.505	1.40	1.52	0.913	1.237	0.643	1.34	1.34	0.433	0.879	0.84	0.716	0.704	0.946	0.828	0.647	0.171	0.479	0.398	0.723
Gd	1.788	1.676	1.46	3.84	3.93	2.53	4.078	1.80	3.78	3.78	1.13	2.56	2.65	2.27	2.28	3.24	2.67	2.7	0.608	1.59	1.29	2.17
Tb	0.375	0.351	0.303	0.579	0.600	0.413	0.588	0.345	0.579	0.542	0.236	0.507	0.495	0.455	0.415	0.622	0.475	0.417	0.122	0.269	0.234	0.428
Dy	2.44	2.21	2.39	3.72	3.77	2.92	3.47	2.68	3.50	3.49	1.98	3.51	3.44	3.19	3.12	4.49	3.39	2.98	0.913	2.02	2.43	3.23
Ho	0.555	0.528	0.556	0.856	0.800	0.605	0.692	0.612	0.808	0.777	0.436	0.837	0.796	0.756	0.713	1.09	0.826	0.73	0.235	0.487	0.544	0.721
Er	1.46	1.36	1.50	2.14	2.15	1.69	1.76	1.68	1.96	2.03	1.24	2.19	2.07	1.91	1.88	2.88	2.11	1.97	0.669	1.23	1.48	2.01
Tm	0.257	0.234	0.257	0.335	0.352	0.272	0.271	0.281	0.319	0.304	0.205	0.311	0.341	0.307	0.29	0.474	0.334	0.338	0.121	0.204	0.248	0.344
Yb	1.42	1.39	1.54	2.10	2.10	1.65	1.65	1.56	1.98	1.93	1.21	2.2	2.02	1.87	1.79	2.77	2.26	2.07	0.849	1.36	1.47	2.02
Lu	0.215	0.201	0.222	0.362	0.320	0.250	0.231	0.231	0.325	0.318	0.190	0.352	0.338	0.322	0.284	0.46	0.339	0.332	0.143	0.218	0.223	0.292
Hf	1.13	0.765	0.816	2.07	2.37	1.42	1.89	0.914	1.91	1.86	0.533	1.57	1.49	1.2	1.21	1.82	1.48	1.12	0.731	0.64	0.72	1.18
Ta	0.044	0.038	0.028	0.140	0.211	0.096	0.197	0.036	0.139	0.155	0.019	0.188	0.189	0.099	0.098	0.08	0.161	0.031	0.077	0.03	0.357	0.039
Pb	1.11	4.36	1.87	3.87	14.5	5.48	3.73	3.88	4.98	7.71	0.797	2.05	3.63	3.29	1.41	3.68	1.6	5.47	1.97	6.87	1.16	4.66
Th	0.140	0.165	0.100	2.76	7.20	4.27	4.18	0.263	3.17	3.10	0.083	0.302	0.263	0.165	0.11	0.09	0.186	0.213	0.238	0.09	0.05	0.371
U	0.129	0.098	0.094	0.816	1.53	1.01	1.18	0.434	0.514	0.924	0.066	0.152	0.231	0.573	0.12	0.056	0.06	0.141	0.208	0.062	0.04	0.12

EVOLUTION OF THE NAIN-BAFT BACK-ARC BASIN THROUGH TIME

The first K-Ar ages performed on amphibole grains from gabbros and amphibolites yielded ages ranging from 67 and 113 Ma (Table 5). These ages are somewhat widespread with a high uncertainty, due to the nature of the amphiboles, partly transformed into actinolite and sometimes into chlorite. The best defined ages are comprised between Aptian-Albian to Cenomanian-Turonian (middle Cretaceous) and in Senonian-Maestrichtian (Late Cretaceous). The well-defined ages (middle to Late Cretaceous) are in agreement with the ages obtained from the microfaunas of the Nain-Baft pelagic limestones (e.g., Davoudzadeh, 1972; Dimitrijevic, 1973). Therefore the birth and evolution of the Nain-Baft back arc basin can be ascribed to the middle Cretaceous. This basin underwent extension with carbonate sedimentation until the Late Cretaceous, as evidenced by the presence of the Upper Cretaceous pelagic limestones. The Early Paleocene represented the closing time of the Nain-Baft basin, favored by sedimentation of the basal brecciated sediments and detritic limestones of Middle Paleocene to Early Eocene age. The southern part of the Nain-Baft basin was tectonically active through the Late Cretaceous, as testified by the presence of volcanic breccias in the Baft complex, stratigraphically overlain by a thick sequence of pelagic limestones.

DISCUSSION AND CONCLUSION

Following oblique subduction of the Tethyan Ocean, during the middle Cretaceous (Agard et al., 2006), a narrow transtensional back-arc basin started to open, along large transcurrent faults, in the active margin of the Iranian continent. The lack of pelagic sediments older than Senonian, and the K-Ar ages are evidence for a middle Cretaceous age of the back-arc spreading. This event was probably the result of anticlockwise rotation of the Lut block (Soffel and Forster, 1984; Soffel et al., 1996). Depletion in HFSE and enrichment in LILE are the peculiar properties of lavas that were erupted in the back-arc basin. The lavas of the Nain-Baft ophiolites are characterized by both calc-alkaline and island-arc tholeiitic signature. Calc-alkaline affinity increases from the Nain complex into the Baft ophiolite. This change and evolution through the lavas is probably related to various degrees of contribution of the slab in the mantle source(s) of these lavas. Therefore, an inhomogeneous slab with high dip in the north (in the case of the Nain ophiolite) and low dip in the south (Baft ophiolite) is thought to be the main agent of these variations.

The position of the Nain-Baft Cretaceous back-arc basins to the north of the Upper Triassic-Jurassic marginal basins of the Esfandagheh region including the Soghan, Sikhoran and Kahnuj complexes (Ghasemi et al., 2002; Kananian et al., 2002; Ahmadipour et al., 2003) indicates the alternance of extension followed by intensive erosion and compression of the active margin of the Iranian continent (the Sanandaj-Sirjan zone), reflecting strong changes in the subduction regime during the middle Cretaceous. Using the isotopic dates and an evaluation of the original distances between the arcs (the Sanandaj-Sirjan and the Urumieh-Dokhtar arcs) and marginal basins (the Esfandagheh and the Nain-Baft marginal basins) from Late Triassic to Cretaceous, we estimate the global migration of the subduction to the north at a rate between 2 to 5 mm/year.

ACKNOWLEDGMENTS

This study was financially supported by the French CNRS, the Cultural Service of the French Embassy at Tehran and by the Iranian Ministry of Sciences, Research and Technology. We are deeply indebted to Dr. Blanchy and Dr. Douamel who made easy this research. R. Boutin and R. Thuizat at ULP have greatly contributed respectively to the whole rock analysis and age determination at Louis Pasteur University. The authors are truly grateful to Prof. Sergio Rocchi for critical reviews and helpful suggestions.

REFERENCES

Agard P., Monie P., Gerber W., Omrani J., Molinaro M., Meyer B., Labrousse L., Vrielynck B., Jolivet L. and Yamato P., 2006. Transient, synobduction exhumation of Zagros blueschists inferred from P-T, deformation, time, and kinematic constraints: Implications for Neotethyan wedge dynamics. J. Geophys. Res., 111: B11401, doi: 10.1029/2005JB004103.

Ahmadipour H., Sabzehi M., Whitechurch H., Rastad E. and Emami M.H., 2003. Soghan complex as an evidence for paleospreading center and mantle diapirism in Sanandaj-Sirjan zone (south-east Iran). J. Sci., Islamic Republic Iran, 14 (2): 157-172.

Arvin M. and Robinson P.T., 1994. The petrogenesis and tectonic setting of lavas from the Baft ophiolitic mélange, southwest of Kerman, Iran. Can. J. Earth Sci., 31: 824-834.

Arvin M. and Shokri E., 1997. Genesis and eruptive environment of basalts from the Gogher ophiolitic mélange, southwest of Kerman, Iran. Ofioliti, 22: 175-182.

Berberian F. and Berberian M., 1981. Tectono-plutonic episodes in Iran. In: H.K. Gupta and F.M. Delany (Eds.), Zagros, Hindukosh, Himalaya geodynamic evolution. Am. Geophys. Union, Washington, p. 5-32.

Berberian M. and King G.C.P., 1981. Towards a paleogeography and tectonic evolution of Iran. Can. J. Earth Sci., 18: 210-265.

Davoudzadeh M., 1972. Geology and petrography of the area north of Nain, Central Iran. Geol. Surv. Iran, Rep., p. 14.

Desmons J. and Beccaluva L., 1983. Mid-ocean ridge and island arc affinities in ophiolites from Iran: paleographic implications. Chem. Geol., 39: 39-63.

Dimitrijevic M.D., 1973; Geology of Kerman Region, Geol. Surv. Iran, Yu/52.

Frenzel G., Muhe R. and Stoffers P., 1990. Petrology of the volcanic rocks from the Lau Basin, southwest Pacific. Geol. Jb., 92: 395-479.

Ghasemi H., Juteau T., Bellon H., Sabzehi M., Whitechurch H. and Ricou L.E., 2002. The mafic-ultramafic complex of Sikhoran (central Iran): a polygenetic ophiolite complex. C.R. Geosci., 334: 431-438.

Hawkesworth C.J., Hergt J.M., McDermott F. and Ellam R.M., 1991. Destructive margin magmatism and the contributions from the mantle wedge and subducted crust. Austral. J. Earth Sci.,38: 577-594.

Kananian A., Juteau T., Bellon H., Darvishzadeh A., Sabzehi M., Whitechurch H. and Ricou L.E., 2001. The ophiolite massif of Kahnuj (western Makran, southern Iran): new geological and geochronological data. C.R. Acad. Sci. Paris, 332: 543-552.

Le Bas M.J., Le Maitre R.W., Streckeisen A. and Zanettin B., 1986. A chemical classification of volcanic rocks based on the total alkali-silica diagram. J. Petrol., 27: 745-750.

McClay K.R., Whitehouse P.S., Dooley T. and Richards M., 2004. 3D evolution of fold and thrust belts formed by oblique convergence. Marine Petrol. Geol., 21: 857-877.

McCulloch M.T. and Gamble J.A., 1991. Geochemical and geodynamical constraints on subduction zone magmatism. Earth Planet. Sci. Lett., 102: 358-375.

McDonough W.F. and Sun S.S., 1995. The composition of the Earth. Chem. Geol., 120: 223-253.

Montigny R., 1989. The conventional potassium-argon method. In: E. Roth and B. Poty (Eds.), Nuclear methods of dating. CEA, Paris, p. 295-324.

Ricou L.E., 1994. Tethys reconstructed: plates, continental fragments and their boundaries since 260 Ma from Central America to South-eastern Asia. Geodyn. Acta, 7: 169-218.

Saunders A. and Tarney J., 1991. Back-arc basins. In: P.A. Floyd (Ed.), Oceanic basalts. Blackie and Son Ltd., p. 219-263.

Shafaii Moghadam H., Rahgoshay M., Whitechurch H. and Montigny R., 2007. A geochemical scenario for evolution of the Nain-Baft back-arc basin. Goldschmidt Conference Abstr., p. A920.

Shahabpour J., 2005. Tectonic evolution of the orogenic belt in the region located between Kerman and Neyriz. J. Asian Earth Sci., 24: 405-417

Soffel H.C. and Forster H., 1984. Polar wander path of the central-east Iran microplate including new results. N. Jahrb. Geol. Palaeont. Abh., 168: 165-172.

Soffel H.C., Davoudzadeh M., Rolf C. and Schmidt S., 1996. New Palaeomagnetic data from central Iran and a Triassic palaeoreconstruction. Geol. Runds., 85: 293-302.

Stern R.J., Lin P.N., Morris J.D., Jackson M.C., Fryer P., Bloomer S.H. and Ito E., 1990. Enriched back-arc basin basalts from the northern Mariana Trough: implications for the magmatic evolution of back-arc basins. Earth Planet. Sci. Lett., 100: 210-225.

Stocklin J., Eftekhar-Nezhad J. and Hushmandzadeh A., 1972. Central Lut reconnaissance, East Iran. Geol. Surv. Iran, Rep., 22.

Taylor B. and Martinez F., 2003. Back-arc basin basalt systematics. Earth Planet. Sci. Lett., 210: 481-497.

Wood D.A., 1980. The application of a Th-Hf-Ta diagram to problems of tectonomagmatic classification and to establishing the nature of crustal contamination of basaltic lavas of the British Tertiary Volcanic Province. Earth Planet. Sci. Lett., 50: 11-30.

Received, November 22, 2007
Accepted, October 30, 2008